Available online at www.sciencedirect.com

ScienceDirect

Journal of Magnesium and Alloys 12 (2024) 608–624

www.elsevier.com/locate/jma

Full Length Article

The influence of yttrium and manganese additions on the degradation and biocompatibility of magnesium-zinc-based alloys: *In vitro* and *in vivo* studies

Lei Shi[a,1], Yang Yan[b,c,d,1], Chun-sheng Shao[a], Kun Yu[b,c], Bo Zhang[a], Liang-jian Chen[a,b,*]

[a] *Third Xiangya Hospital, Central South University, Changsha 410013, China*
[b] *State Key Laboratory of Powder Metallurgy, Central South University, Changsha 410083, China*
[c] *School of Materials Science and Engineering, Central South University, Changsha 410083, China*
[d] *Department of Mechanical Engineering, City University of Hong Kong, Hong Kong, China*

Received 15 September 2021; received in revised form 29 April 2022; accepted 3 June 2022
Available online 29 July 2022

Abstract

The repair and regeneration of bone defects are highly challenging orthopedic problems. Recently, Mg-based implants have gained popularity due to their unique biodegradation and elastic modulus similar to that of human bone. The aim of our study is to develop a magnesium alloy with a controllable degradation that can closely match bone tissue to help injuries heal *in vivo* and avoid cytotoxicity caused by a sudden increase in ion concentration. In this study, we prepared and modified Mg-3 Zn, Mg-3Zn-1Y, and Mg-2Zn-1Mn by hot extrusion, and used Mg-2.5Y-2.5Nd was as a control. We then investigated the effect of additions of Y and Mn on alloys' properties. Our results show that Mn and Y can improve not only compression strength but also corrosion resistance. The alloy Mg-2Zn-1Mn demonstrated good cytocompatibility *in vitro*, and for this reason we selected it for implantation *in vivo*. The degraded Mg-2Zn-1Mn implanted a bone defect area did not cause obvious rejection and inflammatory reaction, and the degradation products left no signs of damage to the heart, liver, kidney, or brain. Furthermore, we find that Mg-2Zn-1Mn can promote an osteoinductive response *in vivo* and the formation of bone regeneration.

Keywords: Magnesium alloy; Biodegradation; Biocompatibility; Bone regeneration; Bone defect repair.

1. Introduction

In order to be considered for applications in bone repair, a biomaterial needs to have good osteoconduction, good osteoinduction, and good osteogenicity [1–3]. Load-bearing orthopedic fields also require that implants have suitable mechanical properties [4]. Major bone repair implants contain autologous bones, ceramics (HA and β-TCP), polymers, Ti-based and stainless steel alloys [5,6]. However, autologous bones may form secondary bone defects at the donor site, and ceramics and polymers cannot provide sufficient mechanical strength [7,8]. In addition, the elastic modulus of Ti-based alloys and stainless steel is much higher than that of human bone, which can cause a stress shield effect [9].

Due to favorable biodegradability and strength, biodegradable metallic implants (Fe-based, Zn-based, and Mg-based implants) are receiving more attention in the search to find an implant that exhibits a suitable biodegradation rate that can satisfy the whole bone repair process [10]. This means a good biodegradable metallic implant must provide sufficient strength during the bone healing period but be gradually absorbed after implantation for a certain time (no less than 12 weeks) with no toxic side effects on human body [4].

* Corresponding author at: Third Xiangya Hospital, Central South University, Changsha 410013, China.
E-mail address: jian007040@sina.com (L.-j. Chen).
[1] These two authors should be considered equal first authors.

https://doi.org/10.1016/j.jma.2022.06.010

Iron-based implants corrode excessively and generate harmful corrosion byproducts that can accumulate in the arteries [11]. With zinc, Zn^{2+} ions might hinder cell adhesion, and Zn-based implants' mechanical properties are less than ideal [12,13].

Compared to natural cortical bone, however, magnesium has a similar elastic modulus and comparative strength [2,14]. Magnesium has a vital role in adhesion and proliferation of osteoblasts, and its degradation byproduct does not cause an obvious inflammatory response [15,16]. Thus, Mg-based implants have great potential to become the ideal candidate material for bone defect repair applications. However, magnesium does show a high degradation rate in a human environment, which can cause adverse effects such as rapid loss of an implant's mechanical integrity, excessive hydrogen gas bubbles, and accumulation of high pH value chemicals. These effects induce cytotoxicity and an increase in overall alkalinity which can interfere with cell growth and tissue healing, potentially limiting Mg-based implants' clinical use [17–19]. One way to build upon the benefits of Mg-based alloys and reduce their drawbacks is to look to Mg-Zn alloys.

Recently, Zn are considered to be promising for enhancing corrosion resistance and strength of Mg-based alloys. The addition of Zn can effectively refine the crystal grains and significantly improve the mechanical strength of magnesium alloys. At the same time, the presence of Zn can improve the stability of the passivation film of magnesium during the corrosion process, thereby improving the corrosion resistance of magnesium alloys [20]. In addition, Zn is also an essential trace element for the human body, and it is not biologically toxic when added in an appropriate amount [21]. Moreover, Moreover, manganese (Mn) is an effective element to refine the grain size of the microstructure of Mg alloys, and improves these alloys' mechanical properties. Mn can form high melting point compounds with impurities in magnesium alloy (mainly Fe) during the smelting process, and then be removed from the smelting process, thereby reducing the content of Fe impurities in the Mg matrix, which is very important for the corrosion resistance of magnesium alloys [22]. In addition, The addition of Mn can also enhance Mg alloys' corrosion resistance by binding the normal Mg corrosion byproduct with manganese oxide, acting as a barrier against Cl^- invasion [23]. Furthermore, yttrium (Y) addition in appropriate content could refine the grain structure with I-phase, strengthening the alloy, and when the Zn/Y ratio is 2.5, the strength of the Mg-Zn-Y alloy reaches its highest value [24]. At the same time, related studies have found that Y-containing magnesium alloys will produce a Y2O3 oxide protective film during the corrosion process, thereby improving the corrosion resistance of magnesium alloys [25]. However, Micro-galvanic cells have been shown to form on the interface between the α-Mg matrix and LPSO phase in Mg-Zn-Y alloys, resulting in initial corrosion that then leads to further corrosion over time [26]. Therefore, in this study, three elements of Zn, Mn, and Y were selected to explore the influence of different composition ratios on the mechanical properties and corrosion resistance of magnesium alloys.

This study examines Mg-3Zn, Mg-3Zn-1Y, Mg-2Zn-1Mn and Mg-2.5Y-2.5Nd alloys' *in vitro* corrosion behavior and cytotoxicity. After careful analysis we selected the Mg-2Zn-1Mn alloy for humerus implantation in rabbits to study its biocompatibility *in vivo* and its effect on bone defect healing. The purpose of this paper is to provide a theoretical basis and guidance for the research and development of new Mg-based alloys.

2. Materials and methods

2.1. Preparation of magnesium alloys

We prepared Mg-3 Zn, Mg-3Zn-1Y, Mg-2Zn-1Mn and Mg-2.5Y-2.5Nd (Wt.%) alloys from pure magnesium (99.99%), pure zinc (99.99%), and Mg-30%Y, Mg-28%Nd, and Mg-5%Mn master alloys. A preheated magnesium ingot was heated and melted in a resistance furnace at 750 °C, and then crushed zinc and Mg-Y master alloy were quickly submerged below the metal liquid surface. After melting, the liquid metal was stirred evenly, when the furnace temperature was dropped to 690 °C, we stirred it again and removing the scum on the melt surface. We then cast it into a preheated metal mold at a temperature of approximately 200 °C. After demolding, the magnesium-based alloy ingots were machined by turning and hot extrusion, and we finally obtained our samples of four kinds of magnesium-based alloys. The chemical composition of the experimental alloy is listed in Table 1. The sample size for our immersion test is 10 mm × 10 mm × 10 mm and for our cytotoxicity test is Φ 6 mm × 5 mm. The size for the animal implantation test is Φ 5.8 mm × 7.8 mm.

2.2. Mechanical tests

We used a universal testing machine (MTS-810) to test the compressive strength and elastic moduli of Mg-3Zn, Mg-3Zn-1Y, Mg-2Zn-1Mn and Mg-2.5Y-2.5Nd.

2.3. Immersion tests

Four groups of Mg-3Zn, Mg-3Zn-1Y, Mg-2Zn-1Mn and Mg-2.5Y-2.5Nd were set up in our experiment, with 3 samples in each group. After polishing the surface of each one with SiC paper, they were each washed by ethanol and distilled water and then air dried. According to the immersion test standard of ASTMG31-72, the samples were weighed and immersed in Ringer's solution (pH = 7.4) and placed in

Table 1
ICP analysis results of the alloys (wt.%).

Alloy	Zn	Mn	Fe	Si	Cr	Mg
Mg-3Zn	2.61	0.008	0.007	0.002	0.003	Bal.
Mg-3Zn-1Mn	2.70	0.86	0.009	0.004	0.005	Bal.
Mg-2Zn-1Mn	1.74	0.95	0.008	0.005	0.007	Bal.
	Y	Nd	Fe	Si	Cr	Mg
Mg-2.5Y-2.5Nd	2.31	2.42	0.006	0.004	0.005	Bal.

a constant temperature water bath at 37 °C (HH-4, Jiangsu Ronghua) for 14d The ratio of the volume of the immersion solution to the surface area of the sample was 20 mL/cm^2.

2.3.1. Weight loss, pH change, and hydrogen evolution detection in vitro

Each sample was dried and weighed at the same time every day, and we plotted each sample's corrosion weight loss curve. The change in the pH value of Ringer's solution in the process of immersion was measured by a PHS3C acidity meter, and we also plotted this change curve. We used an inverted acid burette to collect and measure the H_2 released during immersion on each day. And we calculated the corrosion rate by hydrogen evolution by Eq. (1).

$$CR = \frac{v_H M}{V_m} \tag{1}$$

CR is the corrosion rate, υ_H is the hydrogen evolution rate (mL/cm^2/d), M is the molar mass of magnesium (g/mol), and V_m is the gas molar volume under standard conditions (22.4 L/mol).

2.3.2. Surface corrosion morphology

We observed the corrosion morphology of the Mg-3Zn, Mg-3Zn-1Y, Mg-2Zn-1Mn and Mg-2.5Y-2.5Nd samples after immersion for 14d by scanning electron microscope (SEM, FEI QUANTA-200). The samples were ultrasonically cleaned in 10% CrO_3 solution for 10 min to remove the corrosion byproduct beforehand, and then the samples were ultrasonically cleaned in ethanol for 10 min to clean further the residual corrosion byproducts and CrO_3 solution. We then dried the samples prior to SEM detection.

2.4. In vitro *cell experimentation*

2.4.1. Preparation of extracts

In accordance with the National Standard for Biological Evaluation of Medical Devices GB/T16886.5-2003, we immersed our four sterilized Mg-based alloys in RPMI1640 at 37° C for 72 h with an immersion ratio of 1.25cm^2/ml. The original extract was diluted to 100%, 50%, and 10% concentration gradients, and the pH value and ion concentrations were detected and stored at 4 °C for later use.

2.4.2. Cytotoxicity tests

MG63 cells (provided by the Cell Center of Xiangya Medical School, Central South University, China) were cultured in a RPMI1640 medium in moist air containing 5% CO_2 at 37 °C. Fourteen groups were set: Mg-3Zn (10%,50%,100%), Mg-3Zn-1Y (10%,50%,100%), Mg-2.5Y-2.5Nd (10%,50%,100%), Mg-2Zn-1 M (10%,50%,100%), a negative control group and a positive control group. We prepared six compound holes for each group. The MG63 cells were seeded at a concentration of 5.0 × 104 /ml into 96-well plates (100 μL medium/well) at 37 °C and 5% CO_2 atmosphere for 24 h. After the cells had attached, they were replaced by different concentrations of extracts of the corresponding materials, the negative control group was replaced by fresh medium, and the positive control group was augmented with 10 μl 8 mol/L phenol solution. After incubation for 3d, 20 μl of 5 mg/ml MTT solution (Amresco company) was added and the plates were incubated for 4 h. The supernatant was discarded, and then 150 μl DMSO (SMIGA Company) was added to each well and shaken for 10 min. The OD value was read by enzyme-linked immunosorbent assay (ELX800, Bio-Tek) at 490 nm, and the relative increment rate (RGR) was calculated as follows:

$$\mathrm{RGR}(\%) = (\mathrm{ODtest}/\mathrm{ODnegative}) \times 100\% \tag{2}$$

2.4.3. Cell viability

MC3T3-E1 cells were purchased from The Cell Bank of the Type Culture Collection of Chinese Academy of Sciences (Shanghai, China). Sample extracts that were diluted two, four, and eight times were prepared for further cytotoxicity tests.Alpha modified Eagle's minimum essential medium (MEM, Gbico) supplemented with 10% fetal bovine serum (Gibco) and 1% streptomycin-penicillin (Hyclone) were used as the culture medium for MC3T3-E1 cells. The corresponding sample extracts were prepared as mentioned above. Furthermore, The cells (2 × 10^4/well for MC3T3-E1 cell) were seeded in 24-well plates with corresponding culture medium and cultured at 37 °C with 5% CO_2. After 24 h of incubation, the culture medium was replaced with sample extracts. After 24 h of culture, the original medium was replaced with the conditioned medium of magnesium alloy extract at specific concentrations (100%, 50%, 25%, 12.5% and 6.25%). After culturing for 48 h, respectively, the medium was gently removed. Stained with Calcein-AM/PI double staining kit (Mao Kang,shanghai) for 10 min, observed and photographed under microscope (OM) (Olympus, Japan).

2.4.4. RNA extraction and real-time quantitative PCR (RT-qPCR) analysis

In order to test the effects of Mg-2Zn-1Mn on the bone division of MC3T3-E1, a conditioned medium of specific concentration (100%, 50%, 25%, 12.5%, and 6.25%) magnesium alloy extract is used for subsequent cell culture. MC3T3-E1 was cultured in a 6-well plate (1.5 × 10^{5}cell/well) using a common medium, and incubated for 24 h. Then use conditions to medium substitute, then incubate for 3 days. After osteogenic culture for 3 days, total RNA from MC3T3-E1 was extracted with TRIzol reagent ((Invitrogen, Carlsbad, CA) according to the manufacturer's instructions. RNA concentration was measured by NanoDrop ND-2000 spectrophotometer(NanoDrop technologies, Motchanin, DE, USA). Complementary DNA was synthesized with 1000 ng total RNA using SemiFast^{TM} cDNA Synthesis Kit (Bioline, London, UK). The relative expression of genes was accessed using SYBR Green qPCR Master Mix (Life Technologies) on QuantstudioTM Real-Time PCR machine (Applied Biosystems, Foster City, California, USA). Expression of osteogenic related genes in MC3T3-E1, including alkaline phosphatase (ALP),

type 1collagen (COL1), osteopontin (OPN) and runt-related transcription factor-2 (Runx2) , was tested by qPCR. GAPDH was used as the housekeeping gene. Primer sequence used for qPCR are listed in the supplementary material.

ALP:F:ACTCAGGGCAATGAGGTCAC
R: CACCCGAGTGGTAGTCACAA
COL-1:F:CCTAATGCTGCCTTTTCTGC
R: ATGTCCCAGCAGGATTTGAG
OCN:F:AGACTCCGGCGCTACCTT
R:CTCGTCACAAGCAGGGTTAAG
Runx2:F:GACACTGCCACCTCTGACTT
R:GATGAAATGCTTGGGAACTG
OPN:F:ACCATTCGGATGAGTCTGAT
R: TCAGTCCATAAGCCAAGCTA
GAPDH: F:TGGTGAAGGTCGGTGTGAAC
R:CCATGTAGTTGAGGTCAATGAAGG

2.4.5. Western blot

The MC3T3-E1 were seeded at a density of 1.5×10^5 cells per well for 1 day, then used conditions to medium substitute, then incubated for 3 days. And then lysed using the radioimmunoprecipitation assay (RIPA) lysis buffer (Fdbio Science, China) containing protease and phosphatase inhibitors (ThermoFisher Scientific, USA) for 20 min. After centrifugation, the supernatants were collected and the protein concentrations were determined using the BCA Protein Assay kit (ThermoFisher Scientific, USA). 40 μg of protein for each sample was fractionated by sodium dodecyl sulfate polyacrylamide gel electrophoresis (SDS-PAGE) and transferred to polyvinylidene fluoride (PVDF) membranes. The membranes were blocked with 5% BSA in a TBST buffer and incubated with primary antibodies specific to typical gene ALP and col-1 (affinity 1: 1: 1000), and β-tubulin (affinity 1:5000) at 4 °C overnight, followed by horseradish peroxidase (HRP)-conjugated secondary antibody. Finally, the membranes were imaged using an enhanced chemiluminescence (ECL) kit (Millipore, USA) and a chemiluminescence imaging system.

2.5. In vivo *implantation*

2.5.1. Surgical procedures

Based on the results of the above immersion tests and cytotoxicity tests, we chose Mg-2Zn-1Mn as our implantation material. Twelve adult male New Zealand rabbits (provided by the Animal Experimental Center of Xiangya, Third Hospital of Central South University, China) weighing 2.0–2.5 kg were randomly divided into three batches ($n = 4$, 3 Mg-2Zn-1Mn, and 1 blank control). Before the implantation operation, the rabbits received an intramuscular injection of penicillin G at a dose of 80,000 units in order to prevent infection. The rabbits were then anesthetized with 3% pentobarbital sodium (1.0 ml/kg) intravenously. After general anesthesia, the right humerus of each rabbit was shaved, and the surgical area was further anesthetized with 1% lidocaine and disinfected. Next, we cut open the skin and subcutaneous tissue of the operation area, separated the muscle, cut the periosteum, and fully exposed the middle part of each humerus. Under cooling conditions, an amputated bone defect matching the length of the implant material was prepared for each rabbit in the middle part of the right humerus. The experimental group received Mg-2Zn-1Mn implant material (Φ 5.8 mm × 7.8 mm), and the blank control group did not receive any implant material. Both groups' implants were affixed with a titanium plate and titanium nails. We then rinsed the operation area with normal saline and sutured the muscle and skin layer by layer. After the operation, penicillin G (intramuscular injection, 80,000 U ·bid × 5d) was administered once again in order to prevent infection. The rabbits were harvested at 4 w, 8 w, and 12 w post-operation.

2.5.2. Specimen observation

After the animals were killed, their hearts, livers, kidneys, and brains were removed in order to observe changes in size, shape, color, and texture, and the specimens of the right humerus were taken out to observe their continuity, outline, and morphological changes.

2.5.3. Histological examination of vital organs

Parts of the heart, kidney, liver, and brain tissues were rinsed with normal saline and fixed in 4% formalin, then the pathological sections were stained with HE and observed under a light microscope.

2.5.4. Detection of serum Mg^{2+}, Zn^{2+}, Mn^{2+}

The blood samples of the rabbits were collected before the operation, and 5d, 10d, 15d, 30d, 60d, and 90d after the operation. The concentrations of Mg^{2+}, Zn^{2+}, and Mn^{2+} in serum were detected by ICP mass spectrometry, and we plotted the curve of ion concentration against time.

2.5.5. Imaging of bone specimens and implant samples

X-ray films of the operative area were taken immediately after implantation, and we examined the implantation and the initial condition of the bone defect. We also took X-ray films to observe the degradation and bone healing of the humerus bones at 4 w, 8 w, and 12 w. The humerus specimens of the 12 w implantation group were examined by micro-CT scanning, and the bone healing was observed under three-dimensional reconstruction. The degradation of the sample and the bone regeneration around it were observed on a fracture plane.

The humerus specimens of the 8 w and 12 w implantation groups were examined by microcomputed tomography scanning (ZKKS-MCT-Sharp, Kaisheng Medical, China). Multimodal three-dimensional (3D) visualization software (ZZKS-MicroCT4.1 software, Kaisheng Medical, Guangzhou, China) was used for 3D reconstruction of the images and evaluating new bone volume in the defects by quantifying pixels in these regions. The degradation of the sample and the bone regeneration around it were observed on a fracture plane with CT analysis software (SkyScan, Bruker, Brussels, Belgium, version: 1.14.4). Here, pitting corrosion was not considered due to the limitation of the measuring method. The *in vivo*

degradation rates (r) of the Mg-2Zn-1Mn alloys was calculated based on the volume loss (V). The degradation rate can be described as follows:

$$r = V\rho/t \quad (3)$$

In which ρ is density of the Mg-2Zn-1Mn alloy and t is the degradation time.

2.6. Statistical analysis

Using SPSS 20.0 statistical software for calculations, all data are expressed as mean value ± standard deviation (SD). We also used the software to compute single factor analysis of variance and multi-sample mean SNK-q tests. When $p < 0.05$, we consider a statistic in question provide significant evidence for us to reject the corresponding null hypothesis.

3. Results

3.1. Mechanical properties

Fig. 1 shows optical micrographs of Mg-3 Zn, Mg-3Zn-1Y and Mg-2Zn-1Mn along longitudinal direction. Table 2 shows the comparison of the mechanical properties of Mg-3 Zn, Mg-3Zn-1Y, Mg-2Zn-1Mn and Mg-2.5Y-2.5Nd with human natural bone [27]. The results showed their UCS is inversely proportional to the grain size, which agreed that the main strengthening mechanism of magnesium alloy is fine-grain strengthening. Compared with Ti alloy, the compressive strength and elastic modulus of the four Mg-based alloys are more similar to natural human bone, indicating that the mechanical compatibility is good.

Table 2
Mechanical properties of the 4 sets of Mg-based alloys and human bone.

Material	UCS (MPa)	Modulus (GPa)
Mg-3Zn	119.5	20.3
Mg-3Zn-1Y	162.0	38.1
Mg-2Zn-1Mn	150.5	31.1
Mg-2.5Y-2.5Nd	212.1	42.2
Ti-based alloy [27]	758.0–1117.0	110.0–117.0
Human bone [27]	130.0∼180.0	3.0∼20.0

3.2. In vitro degradation

3.2.1. Weight loss

When Mg-3 Zn, Mg-3Zn-1Y, Mg-2Zn-1Mn and Mg-2.5Y-2.5Nd were in Ringer's solution, the quality of Mg alloy lessens due to corrosion. From Fig. 2, we see that the weight of four groups decreased slightly during the first 3 days. After 3 days, the mass loss of Mg-2.5Y-2.5Nd and Mg-3 Zn was obvious, while the weight loss of Mg-3Zn-1Y and Mg-2Zn-1Mn were not significant, merely fluctuating in a small range

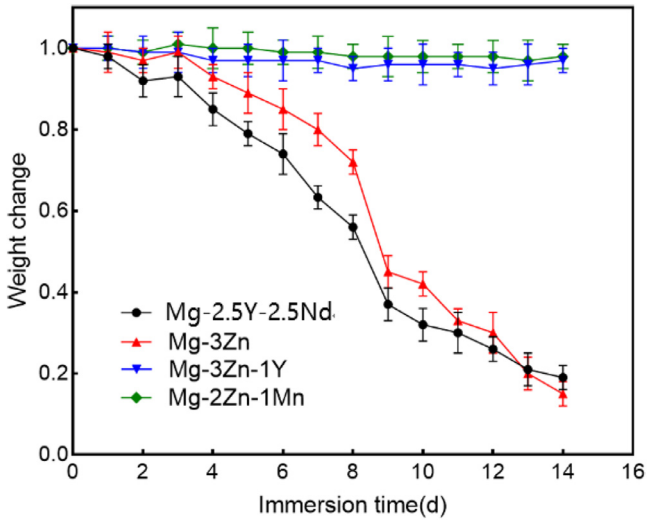

Fig. 2. Weight loss of 4 sets of magnesium based alloys at different time.

from their initial mass. After soaking for 14 days, the quality of Mg-2Zn-1Mn was 99.8% of that before soaking; the quality of Mg-3Zn-1Y was 97.3%, and the quality of Mg-2.5Y-2.5Nd and Mg-3 Zn were only 14.4% and 19.3%, respectively.

3.2.2. Change in pH value of the soaking solution

The corrosion of magnesium alloy in Ringer's solution results in an increase in pH value of the solution. From Fig. 3, we see that the pH value of the soaking solution rose rapidly in the first 2 days. During the first 2 days, the Mg-2.5Y-2.5Nd alloy and Mg-3 Zn groups reach a pH of 9.0, while the Mg-3Zn-1Y and Mg-2Zn-1Mn groups measured 8.5. After that, the pH of the Mg-3 Zn and Mg-2Zn-1Mn groups remained stable until the 14 days. However, after the first 2 days the

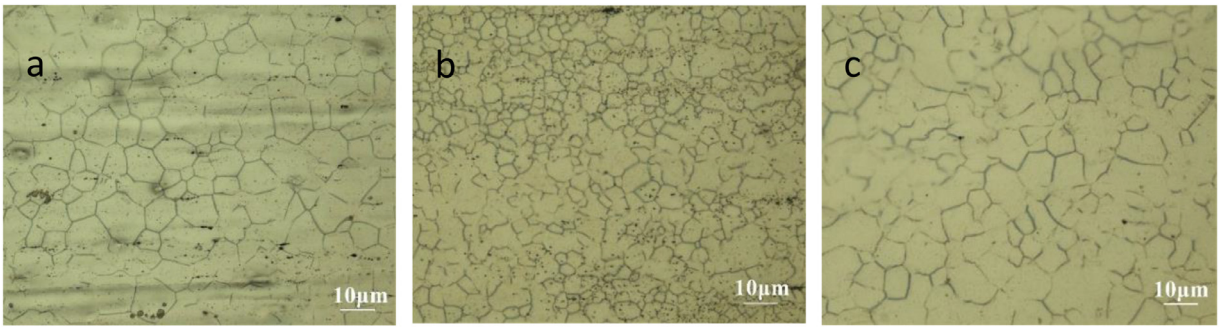

Fig. 1. The optical micrographs of Mg-3Zn (a), Mg-3Zn-1Y (b) and Mg-2Zn-1Mn (c) along longitudinal direction.

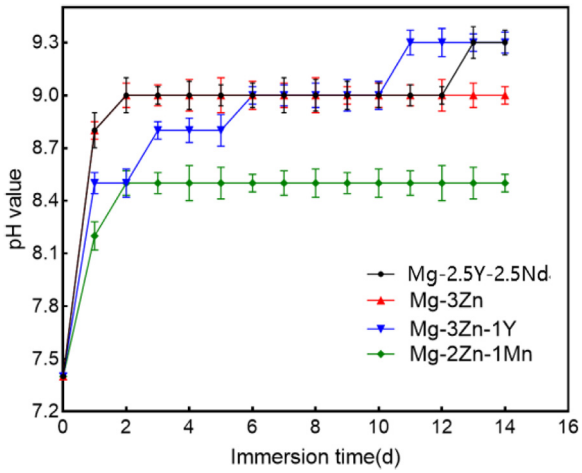

Fig. 3. The pH value of the soaking solution of 4 sets of Mg-based alloys at different times.

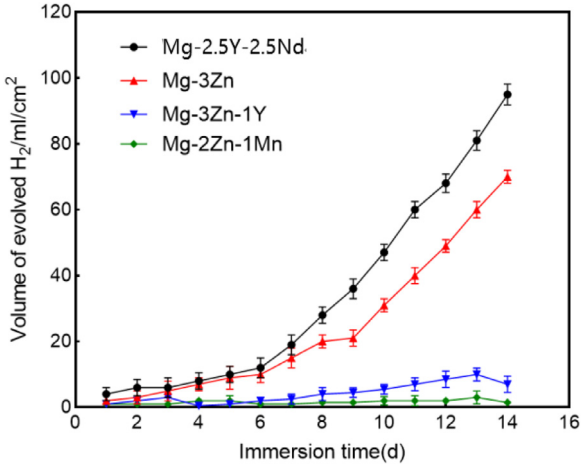

Fig. 4. Volume of evolved H_2 in 4 sets of Mg-based alloys at different time.

pH value of the Mg-2.5Y-2.5Nd and Mg-3Zn-1Y groups increased gradually and reached 9.3 on the 14d.

3.2.3. Change in hydrogen evolution

Magnesium alloys produce hydrogen during corrosion. Fig. 4 presents the change in the hydrogen evolution amount of four groups of magnesium alloys during Ringer's immersion. During the experiment period of 14 days, the hydrogen evolution of the Mg-2.5Y-2.5Nd group was the highest, and that of the Mg-2Zn-1Mn group was the lowest. The changes in hydrogen evolution in Mg-3Zn-1Y and Mg-2Zn-1Mn groups were gentle and at a low level, and the change in the Mg-2Zn-1Mn group was lower than that in the Mg-3Zn-1Y group. However, the hydrogen evolution of Mg-3Zn and Mg-2.5Y-2.5Nd increased significantly throughout the 14 days and showed no slowing of this trend by the 14 days.

3.2.4. Rate of corrosion

The reaction of magnesium corrosion is as follows.

Anodic reaction:

$$Mg - 2e^- \rightarrow Mg^{2+} \quad (4)$$

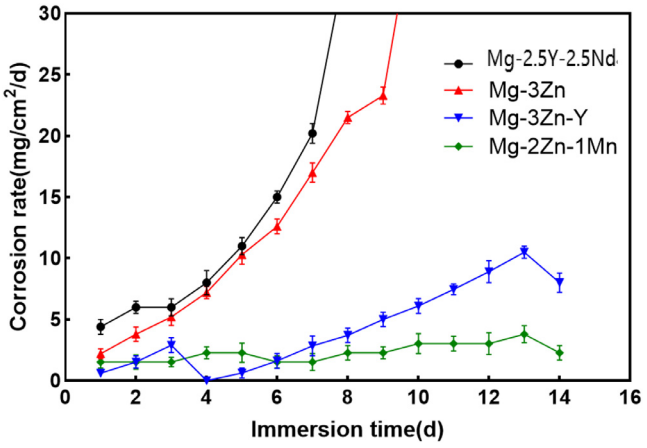

Fig. 5. Corrosion rate of 4 sets of magnesium based alloys at different time.

Cathodic reaction:

$$H_2O + 2e^- \rightarrow H_2 \uparrow + 2OH^- \quad (5)$$

The comparison of corrosion rates of Mg-3Zn, Mg-3Zn-1Y, Mg-2.5Y-2.5Nd, and Mg-2Zn-1Mn is shown in Fig. 5. The corrosion rate of Mg-3Zn and Mg-2.5Y-2.5Nd is obviously higher than that of Mg-2Zn-1Mn, and the corrosion rate of Mg3Zn-1Y is similar to that of Mg-2Zn-1Mn in the first 8 days but then increases to 10.61 mg/cm^2/d. During the 14d period, the corrosion rate of Mg-2Zn-1Mn fluctuated within the range of 1.52∼3.79 mg/cm^2/d.

3.2.5. Corrosion morphology

The SEM images of four sets of Mg-based alloys showed obvious differences in corrosion morphologies (Fig. 6). The Mg-3Zn and Mg-3Zn-1Y alloys had a large number of acicular crystals in clusters on their surfaces (Fig. 6a and b). There were many small cracks and groove defects on the surface of Mg-2.5Y-2.5Nd; the soaking solution can infiltrate into the sample matrix through these cracks and cause deep corrosion (Fig. 6c). Millet deposits could be seen on the surface of Mg-2Zn-1Mn, and there were no obvious cracks or corrosion on the surface of the sample or below it (Fig. 6d).

3.3. In vitro *biocompatibility*

3.3.1. Change in the pH value of the extracts

The pH values of Mg-3 Zn, Mg3Zn-1Y, Mg-2.5Y-2.5Nd, and Mg-2Zn-1Mn after 72 h of extraction from the culture medium are as shown in Table 3. The pH value of Mg-2.5Y-2.5Nd extract was the highest (9.5), while the pH value of Mg-2Zn-1Mn extract was the lowest (8.5). We also observe

Table 3
The pH value of the extracts of 4 sets of Mg-based alloys.

	100%	50%	10%
Mg-3Zn	8.8	8.5	7.5
Mg-3Zn-1Y	9.0	8.5	7.5
Mg-2Zn-1Mn	8.5	8.0	7.5
Mg-2.5Y-2.5Nd	9.5	8.8	7.5

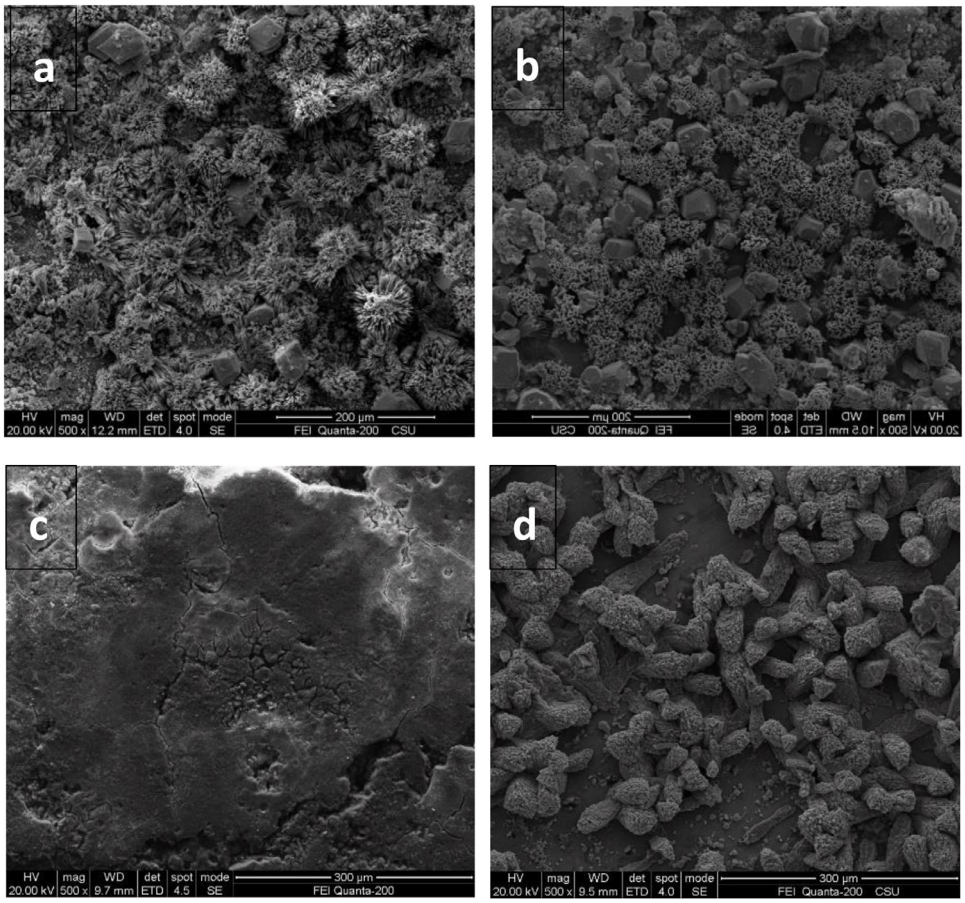

Fig. 6. SEM images of corrosion morphology of 4 sets of Mg-based alloys on the 14th day: (a) Mg-3 Zn; (b) Mg-3Zn-Y; (c) Mg-2.5Y-2.5Nd; (d) Mg-2Zn-1Mn.

that the pH values decreased with an increase in the dilution ratio of the extract. When diluted ten times with the medium, the pH value of the four kinds of alloy extracts was 7.5, which is consistent with the fluctuation ranges of the pH values of human bodily fluids.

3.3.2. Ion concentration of the extracts

We used the chemiluminescence method to detect the Mg^{2+} concentrations in the four groups of 100% extract (Fig. 7). The concentration of Mg^{2+} in the extract of Mg-2.5Y-2.5Nd was the highest, and the lowest concentration was in Mg-2Zn-1Mn. In addition, there is no significant difference in Mg^{2+} concentration between Mg-2.5Y-2.5Nd and Mg-3Zn-1Y extract ($p > 0.05$).

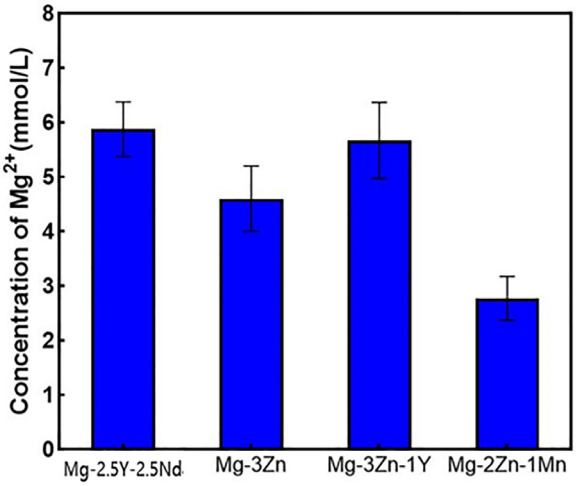

Fig. 7. Concentration of Mg^{2+} in the extracts of 4 sets of Mg-based alloys.

3.3.3. Cytotoxicity

After MG63 cells were cultured with extract for 3 days, we observed the following under inverted phase contrast microscope (Fig. 8): when the concentration of Mg-3Zn, Mg-3Zn-1Y, and Mg-2.5Y-2.5Nd extract was 10%, the number of cells was large, and most of the cells were fusiform or polygonal, which was not significantly different from that of the negative control group (Fig. 8a3, b3, c3). When the concentration of the extract was 50%, the number of cells was less, and the cell volumes began to become smaller and show a jujube nucleus. Some of them had become round and apoptotic (Fig. 8a2, b2, c2). When the concentration of the extract was 100%, the number of cells was obviously reduced. More round dead cells and cell lysis fragments (Fig. 8a1, b1, c1) could be seen. However, when the concentration of the extract of Mg-2Zn-1Mn was 100%, most MG63 cells still grew well (Fig. 8d1), and when the concentration

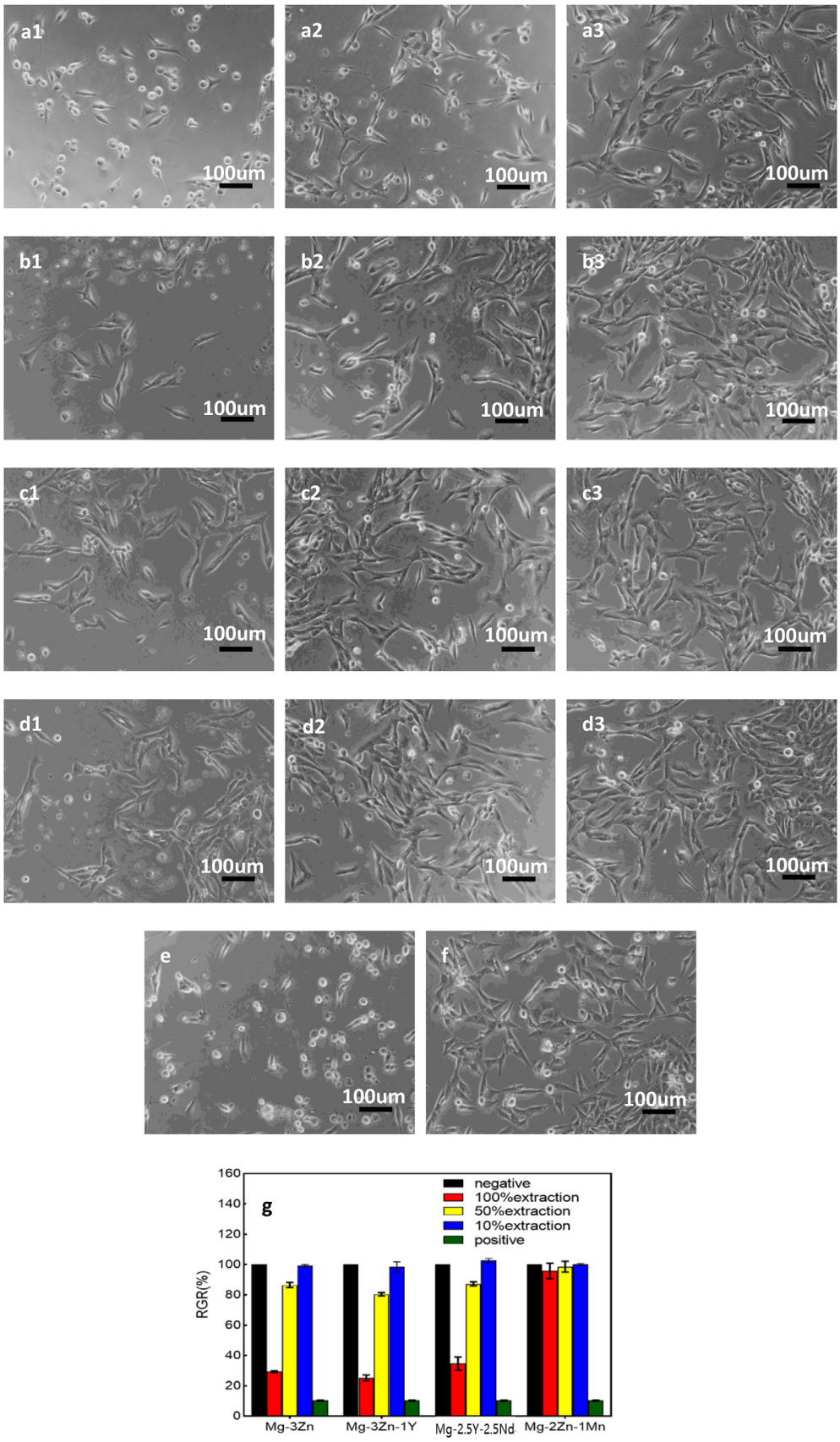

Fig. 8. Cytotoxicity results of the 4 sets of Mg-based alloys: (a) Mg-3Zn: (a1)100%; (a2) 50%; (a3)10%; (b) Mg-3Zn-1Y: (b1) 100%; (b2) 50%; (b3) 10%; (c) Mg-2.5Y-2.5Nd: (c1) 100%; (c2) 50%; (c3) 10%; (d) Mg-2Zn-1Mn: (d1) 100%; (d2) 50%; (d3) 10%; (e) positive control; (f) Negative control; (g) relative growth rate (RGR) of MG63 cells cultured in different extracts.

was 50% and 10%, there was no significant difference in cell growth compared with the negative control group (Fig. 8d2, d3). The cells in the positive control group nearly all died (Fig. 8e) and showed cell cleavage fragments. These results suggest that Mg-2Zn-1Mn has no cytotoxicity to MG63.

We calculated the RGR according to the OD value determined by the MTT method and score a cytotoxicity grade (CTS). The extracts of Mg-3Zn, Mg-3Zn-1Y, and Mg-2.5Y-2.5Nd all showed obvious cytotoxicity when the concentration was 100%. Here the toxicity grade was 3, but the cytotoxicity decreased when the concentration was 50% and 10%, indicating that these were toxic to MG63 cells. However, the cytotoxicity grade of Mg-2Zn-1Mn extract was 0–1 at all concentrations, indicating that the Mg-2Zn-1Mn prepared in this study had no toxicity to MG63 cells and met the cytotoxicity requirements of "materials in the National Standard for Biological Evaluation of Medical Devices GB/T 16,886.5-2003".

3.3.4. In vitro *assessment of impacts of Mg-2Zn-1Mn on osteogenic pathways*

Based on the above-mentioned results, it can be concluded that the cytotoxicity of 100% extract was lower than that of Mg-3Zn, Mg-3Zn-1Y, Mg-2.5Y-2.5Nd. Mg-2Zn-1Mn, the latter possesses higher mechanical properties and a lower degradation rate which is more stable and controllable. Therefore, we chose Mg-2Zn-1Mn to further study the impact of the alloy on cell viability and osteogenic pathways. The MC3T3-E1 cells were cultured in an osteogenic differentiation induction medium containing different concentrations of the Mg-2Zn-1Mn extracts (6.25%, 12.5%, 25%, 50% and 100%), and the cell viability, cell membrane integrity, and osteogenic differentiation were assessed *in vitro*.

Fig. 9 showed the effects of the different concentrations (6.25%, 12.5%, 25%, 50% and 100%) of the Mg-2Zn-1Mn extract on the osteogenic pathways of MC3T3-E1 in terms of cell viability and cell membrane integrity after culturing for 48 h as determined by AO/EB assay. The 6.25% and 12.5% concentration extracts showed promoting effects on cell viability and no apoptotic or necrotic cells. The 50% and 25% concentration extracts showed no significant influence on cell viability and few apoptotic and necrotic cells, the 100% concentration extract showed a number of apoptotic and necrotic cells.

The osteogenic gene expression of the MC3T3-E1 cells after being cultured in different Mg-2Zn 1Mn extract concentrations for 3 days. Fig. 10A–D shows the mRNA levels of the osteoblast differentiation markers, including OPN, RUNX-2,COL-1,ALP; the mRNA expression of OPN in 50% extraction concentration is significantly increased and higher than in other groups; and the mRNA expression of RUNX-2 in 100% and 25% are significantly increased. In addition, there is no significant differences in COL-1 and ALP. Relative expression of osteogenic protein ALP, and COL-1 are significantly increased by Mg-2Zn-1Mn in 6.25% ∼ 50% extract concentration, especially in the groups of 50% and 12.5%.

3.4. In vivo *bone regeneration and biosecurity*

3.4.1. Naked eye observation

The operation process on the 12 New Zealand rabbits went smoothly, and their the postoperative recovery and appetite were good. We observed no cracking and no obvious subcutaneous emphysema in any rabbit. Their wounds all healed well, and their stitches were removed after 10 days. The movement of the rabbits was limited within 1 week after the procedure. After 1 week, their activity was nearly back to normal, and the rabbits could bear weight on their affected front legs one and a half months later. Examination of the operation area showed that at 4 weeks (Sup. 1a1, 1b1), the titanium plates in the blank control group were bent, the bone in the defect area was discontinuous. In the implantation group the alloy samples were partially degraded, the bone defect area was surrounded by a dense fibrous membrane, and some new bone was formed at the broken end of the bones. At 8 weeks (Sup. 1a2, 1b2), we observed callus repair in the defect areas of the blank control group, and could see a small residual sample in two rabbits of the implantation group. The specimen of the third implantation group rabbit was completely degraded, and the bone continuity was restored. At 12 weeks (Sup. 1c1, 1c2), the bones in the blank control group healed completely but had bone enlargement with angular deformity at the healing site. The bone defects in the implantation group had all also healed completely; the appearance of the tibia were nearly the same as those in normal rabbits. The bones at the two ends of the defects were naturally connected, and the color of the new bones was not abnormal.

3.4.2. Pathological examination of vital organs

After 4 weeks, 8 weeks and 12 weeks of implantation, the heart, liver, kidney, and brain of the rabbits were removed for tissue section examination. The cardiac tissue section (Sup. 2) showed that the myocardial fibers gathered into bundles and were arranged neatly, there was a small amount of connective tissue between the myocardial fibers and muscle bundles, and we found no abnormal cardiomyocyte hypertrophy or edema. The liver tissue section (Sup. 3) showed hepatic lobular structure, central venous lumen in the middle of the lobule, and radially arranged hepatic cords and hepatic sinusoids. We found no abnormal hepatocyte degeneration, interstitial fibrosis, and no obvious inflammatory cell infiltration. In the renal tissue section (Sup. 4), there was a large number of different sections, dense and parallel arrangement of tubules in the renal medulla and regular lumen, no abnormal vitreous degeneration or fibrosis, and no obvious inflammatory cell infiltration. The brain tissue section (Sup. 5) revealed that the medulla was light pink, showing pink nerve fibers and deeply stained glial nuclei, with unclear boundaries; there was no cell swelling, gelatinization, or focus of hemorrhage or necrosis. These results suggest that Mg-2Zn-1Mn had no obvious pathogenic effect on the heart, liver, kidney, or brain of the rabbits.

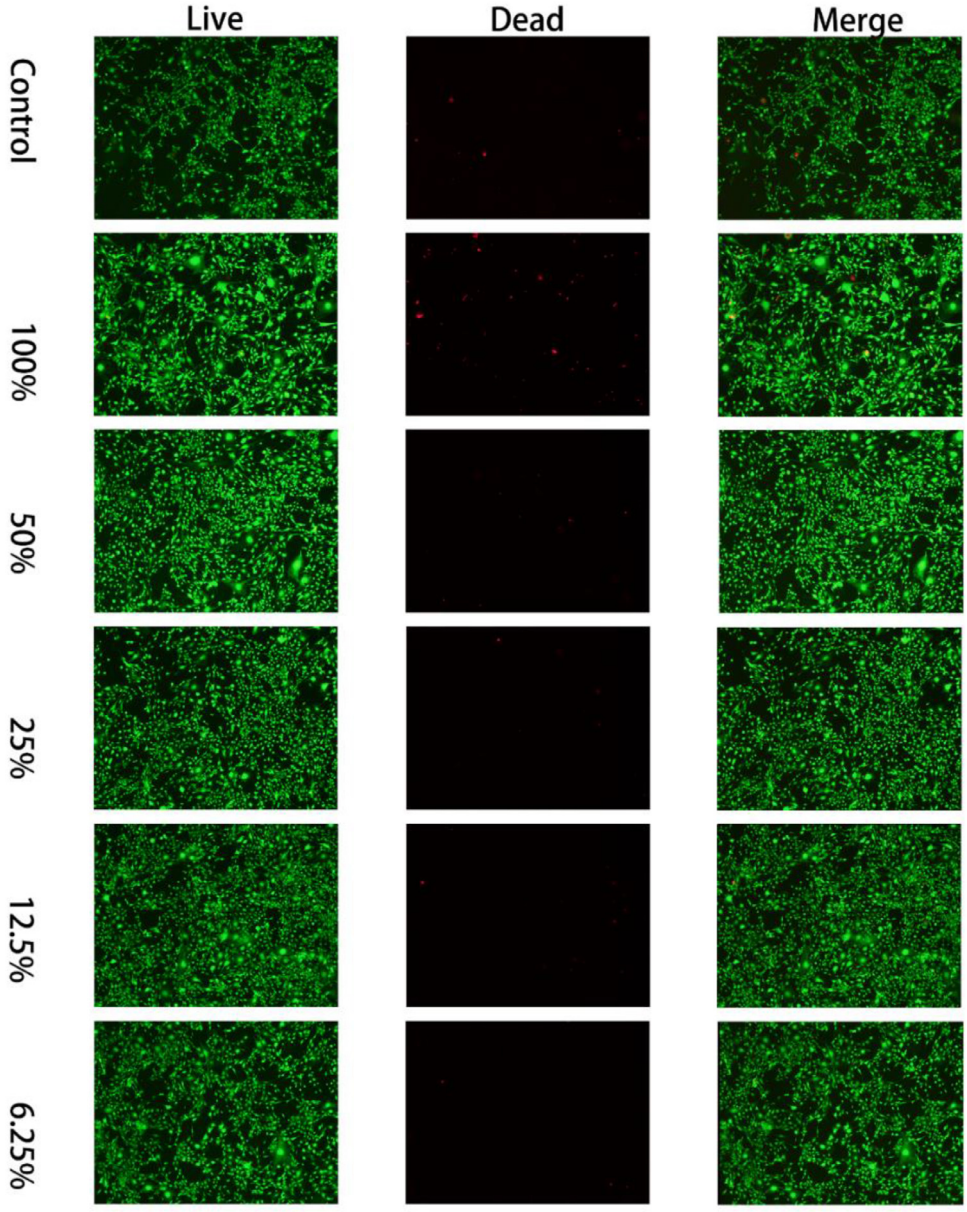

Fig. 9. Effects of different concentrations of the Mg-2Zn-1Mn extract on the cell membrane integrity of MC3T3-E1 cells determined by AO/EB staining.

3.4.3. Serum concentrations of Mg^{2+}, Zn^{2+}, Mn^{2+}

At each time point, the serum concentrations of Mg^{2+}, Zn^{2+}, and Mn^{2+} of the blank control group and Mg-2Zn-1Mn implantation group fluctuated slightly, and the changes in ion concentration are shown in Fig. 11. The concentrations of serum Mg^{2+} and Zn^{2+} in both groups did not exceed the maximum concentration of Mg^{2+} and Zn^{2+} in rabbit serum (Mg^{2+}: 1.66 mmol/L; Zn^{2+}: 170.00 μmol/L) [28]. The concentration of serum Mn^{2+} in the implantation group increased slightly within 5–15 days after operation and then decreased to the same level as that in the blank group.

3.4.4. X-ray and micro-CT examination

The X-ray images taken immediately after the operations showed that the length of the bone defects in the blank group was the same as that in the implantation group, and both groups had their defects located in the middle of the humerus. The materials in the implantation group aligned well with the broken end of the bones (Fig. 12a, b). Four weeks after the procedure, in the blank control group the regular defect areas were deformed and shortened, and some bone formation could be seen around the titanium implant. In the implantation group, however, the titanium plate could be retained, and the degradation of the implant was not obvious (red arrow). There was new bone formation (blue arrow) at the bone ends and callus formation on one side, and the continuity was nearly completely restored (Fig. 12a1, b1). Eight weeks after the operation, a large amount of callus formed and bone continuity recovered in the blank control group, but the outline of the bone cortex was blurred, with uneven bone density. Most of

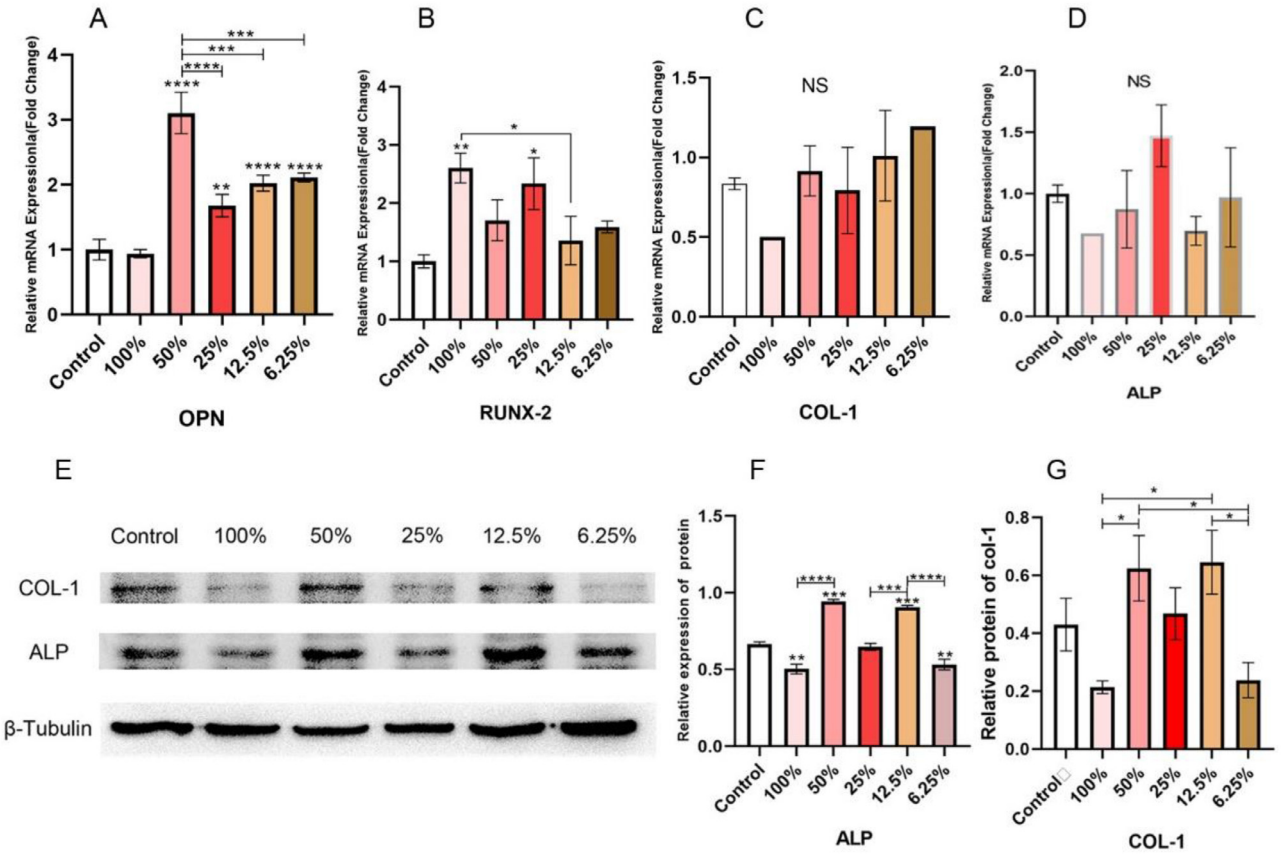

Fig. 10. Expression of osteogenic gene of the MC3T3-E1 cells cultured in different extract concentrations for 3Days. Relative mRNA expression levels of (A) OPN , (B) Runx-2 ,(C) COL-1, (D) ALP. Relative protein expression levels :(E–G) protein levels of ALP and COL-1 determined by immunoblotting. $^{*}p < 0.05$,$^{**}p < 0.01$, $^{***}p < 0.005$, $^{****}p < 0.005$.

the implants in the implantation group were degraded, some of the nondegraded implant materials were located in the center of the defect area, wrapped by new bone, and bone continuity recovered fully (Fig. 12a2, b2). After 12 weeks, the bone mineral density in the defect areas of the blank control group was higher than at 8 weeks, the bone hyperplasia was enlarged, and the angular malformation had healed. In the implantation group, the fixed titanium plate was not deformed, more new bone tissue was formed in the bone defect area (blue arrow), and the bone continuity was restored. The implant also had residual (red arrow) (Fig. 12a3, b3).

The Mg-2Zn-1Mn alloys were implanted into the humerus bone defect of rabbits for 8 weeks and 12 weeks were scanned and reconstructed by micro-CT, and the degradation of the implants (Red arrow) and the healing of bone defects (Blue arrow) were observed (Fig. 13).

It can be seen from Fig. 13A that the formation of a large amount of bone callus and new bone occurred after the alloy was implanted at the defect site for 8 to 12 weeks; the callus was transformed and shaped, and the bone continuity in the humeral bone defect area was gradually restored. Finally, images in 12 W showed that the bone defect healed well. And most of the implant degraded, leaving an intraosseous cavity surrounded by a large number of new bone tissue. In detail, the new bone density was higher, and the new bone tissue was completely connected with the host bone and wrapped in the outer layer of the implant.

By analyzing the quantity and quality of the newly formed bone in the 8 W and 12 W defect areas, and the volume of the implant, it was found that with the extension of the implantation time, the volume loss of the implant increased, while the amount of newly formed bone tissue increased. And the thickness of trabecular bone and the ratio of new bone area to volume were not significantly different.

Fig. 13B–E. At the same time, it was also found that at 12 W, the amount of implant degradation increased, and the space generated by the degradation was not filled with new bone, but was in a low-density image, which may be due to the increased accumulation of degradation products, which made the local osteogenic microenvironment unfavorable for osteogenesis.

4. Discussion

4.1. Mechanical properties

Due to the extrusion ratio used in this experiment was relatively low, resulting in the strength of the alloys were not superior high, compare to other study work. However, the

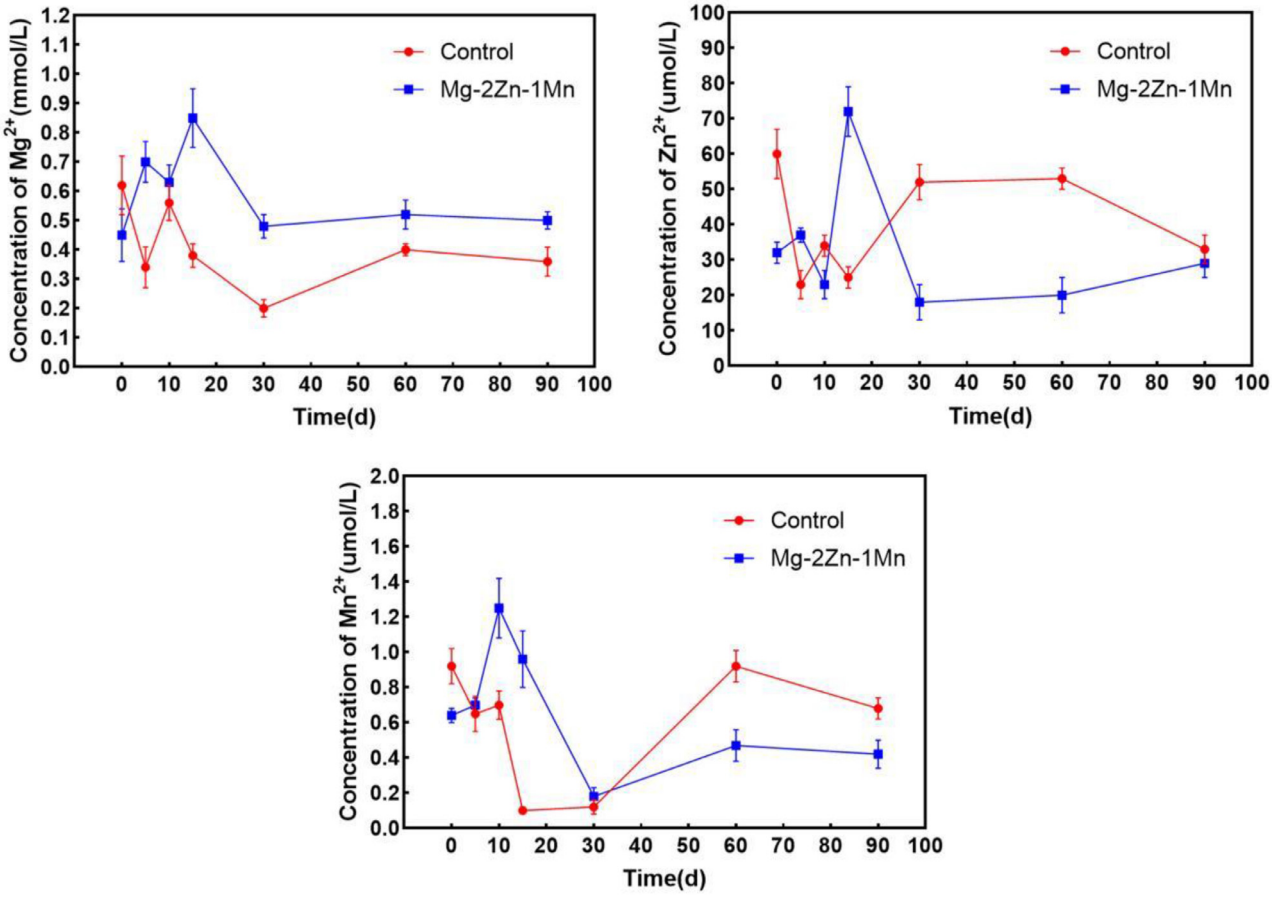

Fig. 11. Concentration of serum Mg^{2+}, Zn^{2+} and Mn^{2+} at different times.

elastic modulus similar to that of human bone make them worthy of further research.

The strength of pure magnesium in the cast state is very low, only ~30 MPa, and its elastic modulus is about 45 GPa. The compressive strength and elastic modulus of the four sets of magnesium alloys prepared in this study are close to those of human bone and have good mechanical compatibility with bone (Table 2). These excellent mechanical properties can be attributed to the following factors. The introduction of zinc or rare earth elements such as yttrium and gadolinium into the magnesium matrix can produce solid solution strengthening and significantly enhance the strength of the alloy [29,30]. However, when the zinc content is less than 3%, the strength of the alloy can continue to increase; when above 3%, the intermetallic precipitate can become a crack initiation site and reduce the ductility of the alloy [31]. The neodymium in Mg-2.5Y-2.5Nd enhances the mechanical properties of alloying mainly through the formation of intermetallic phases between grain boundaries [32,33]. The compressive strength of Mg-3Zn-1Y prepared in this study is 42.5 MPa higher than that of Mg-3Zn, while Mg-2.5Y-2.5Nd shows the highest compressive strength and elastic modulus, which also indicates that the introduction of rare earth elements can strengthen the mechanical properties of Mg-based alloys. Zinc can also refine the grains of Mg-Mn alloy and improve its yield strength.

4.2. In vitro *corrosion*

Rapid corrosion is a defect of magnesium alloy when used as a bone implant. Magnesium react in aqueous solution to produce $Mg(OH)_2$ and H_2. The $Mg(OH)_2$ can be deposited on the surface of the material and act as a relatively protective film [27]. However, in high chlorine (> 30 mmol/L) environments, $Mg(OH)_2$ is easily converted into $MgCl_2$ and loses its protective effect. Zinc can reduce the content of impurity elements such as copper, iron and nickel during smelting, and thus reduce the galvanic corrosion between these impurities and the magnesium matrix [34]. The introduction of manganese into the alloy can form Fe-Mn precipitate, control the content of iron impurities, refine the precipitate product, and increase the creep resistance of the alloy to improve its corrosion resistance. Anderson and Stumpf [35] and Lunder et al. [36] demonstrated that the $MgO/Mg(OH)_2$ on the surface of Mn-containing Mg-based alloys is significant, which can enhance the surface dullness of these alloys. Rosalbino et al. [37] also found enhanced effect of zinc and manganese on the corrosion resistance of Mg-based alloys. Hence, the introduction of zinc and manganese into the magnesium and the increase of zinc and manganese content in the alloy can reduce the surface reactivity of magnesium and increase the forma-

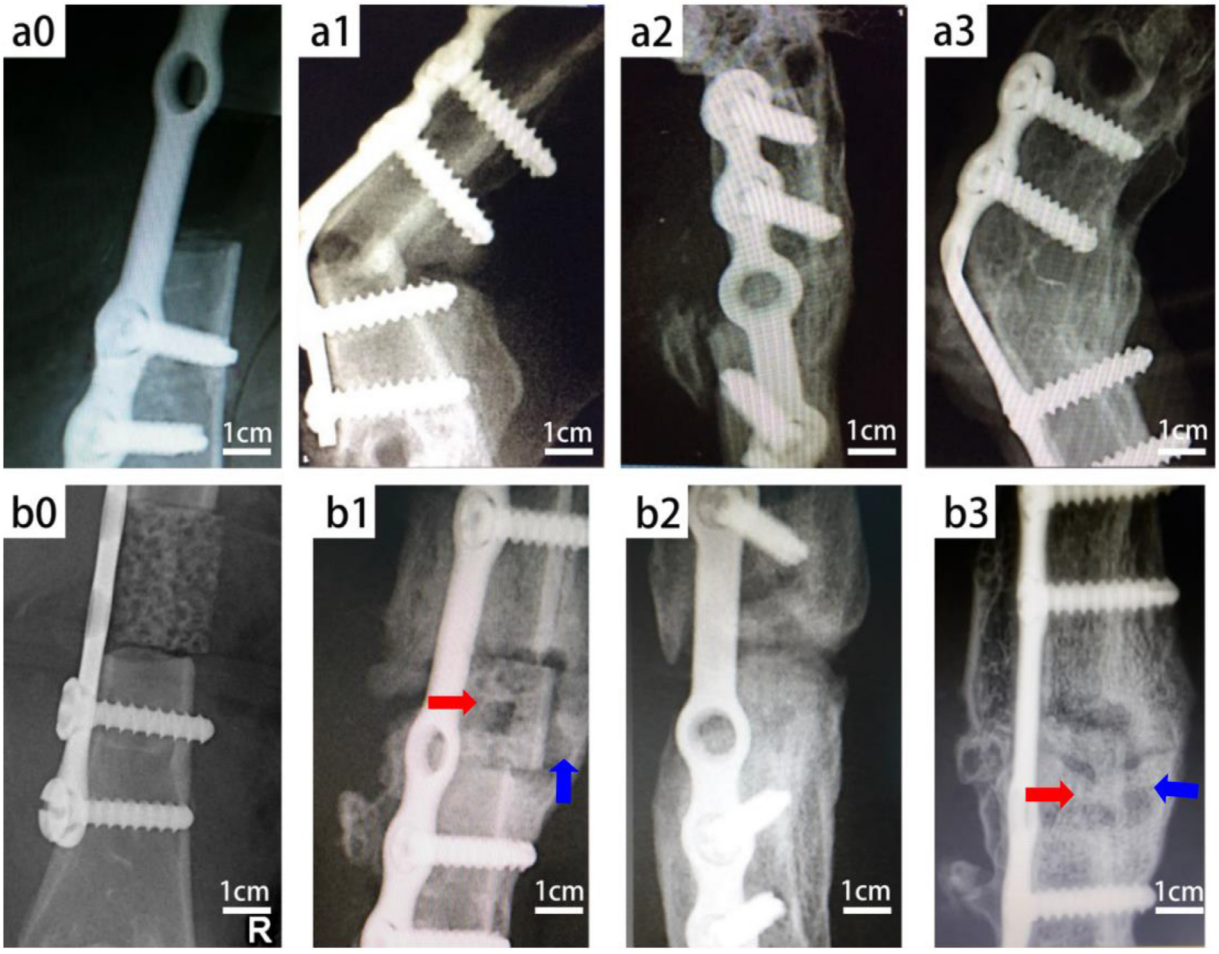

Fig. 12. X-ray images of the operated bone at different time: the blank control: a0, immediately after operation; a1, 4 w; a2, 8 w; a3, 12 w; the experimental group: b0, immediately after operation; b1, 4 w; b2, 8 w; b3, 12 w (For interpretation of the references to color in this figure legend, the reader is referred to the web version of this article.).

tion of degradation products with corrosion protection ability.

The rare earth elements can improve the casting properties of Mg-based alloys; they have precipitation strengthening and solid solution strengthening at room and high temperature. These elements can also improve the creep properties and high temperature tensile properties of Mg-based alloys to improve their corrosion behavior. Among the rare earth elements, yttrium is an effective solid solution hardener with good solubility in magnesium. This can improve the creep properties of the alloy [38]. The solubility of neodymium in magnesium is limited, however, but the introduction of neodymium can significantly enhance the corrosion resistance of Mg-based alloys [39]. Adding a small amount of yttrium and neodymium to Mg-based alloys can improve the microstructure and enhance the corrosion resistance of these alloys. Neodymium can form a protective film containing neodymium oxide on its surface, which also enhances the corrosion resistance of these alloys [40].

Because only Ringer's solution as an electrolyte in the in-vitro test is incomplete, therefore we added the immersion test of Mg-2Zn-1Mn with Hank's solution at 240 h of corrosion. In addition, we added the SEM morphology and EDS energy spectrum analysis after corrosion.

As Fig. 14. Shown, compared to Hank's solution, the alloys showed better corrosion resistance than that in Ringer's solution, which has a great relationship with the formation of calcium-containing corrosion products.

4.3. In vitro *cytotoxicity*

In vitro cytotoxicity tests (Fig. 8) showed that the Mg-2Zn-1Mn prepared in this study had no toxicity to MG63 cells, while Mg-3Zn, Mg-3Zn-1Y, and Mg-2.5Y-2.5Nd showed different degrees of cytotoxicity to MG63 cells. As the concentration of the extracts decreased, the cytotoxicity decreased. Some studies [41] have found that zinc and manganese showed cytotoxicity after 24 h extraction in DMEM. After extraction in HEPES buffer for 1 h, only magnesium showed no cytotoxic reaction. Yttrium is the most toxic of the commonly used rare earth elements (yttrium, gadolinium, and neodymium), but neodymium has good biocompatibility. Studies have found that relatively high concentrations of neodymium can be tolerated by many types of

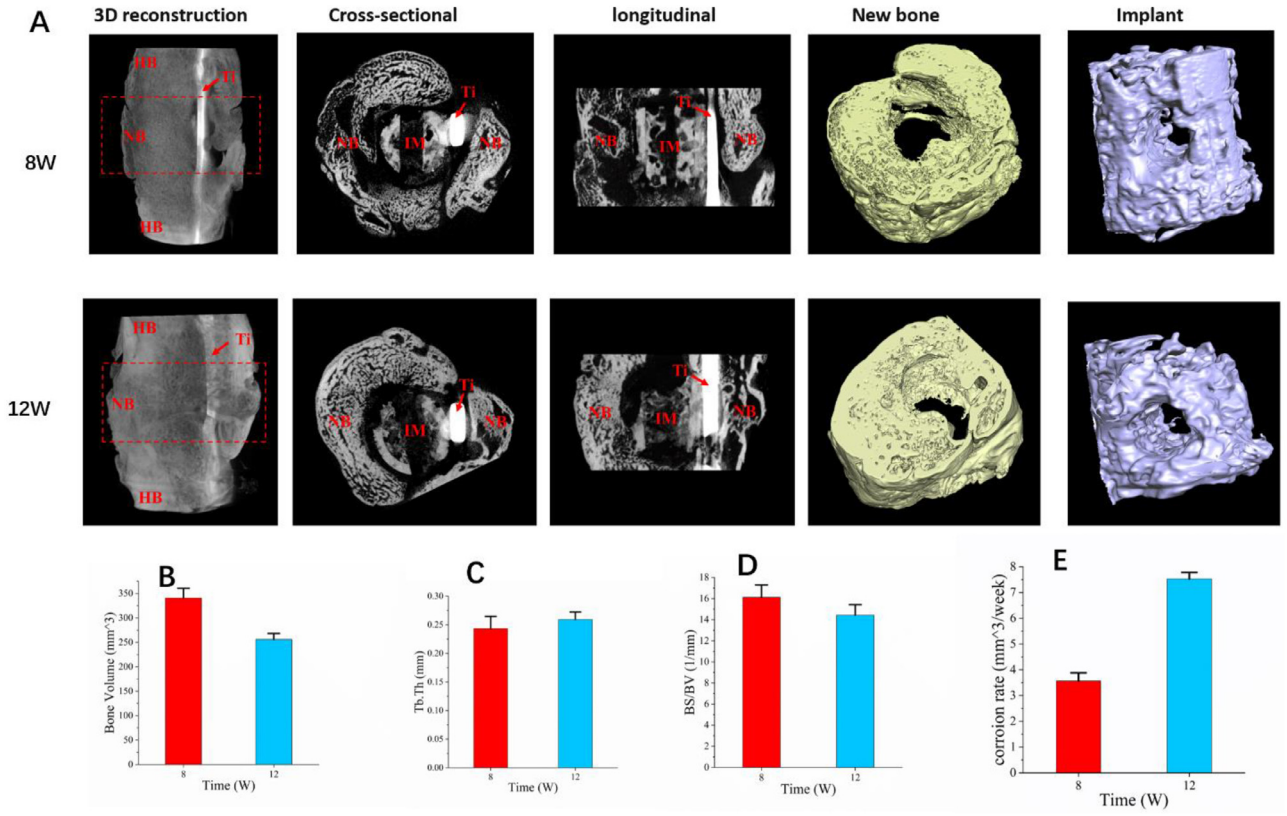

Fig. 13. Effects of Mg-2Zn-1Mn on bone regeneration in defect area after implantation in rabbits for 8 and 12 weeks: (A) 3D reconstruction, longitudinal, cross-sectional, new bone and implant micro-CT images of the implant, NB new bone, HB host bone, IM implant, Ti titanium; (B) new bone volume; (C) trabecular thickness; (D) Bone surface/ volume; (E) *in vivo* degradation rate.

cells [42]. The toxicity of biodegradable materials is also related to their corrosion behavior. The faster the material corrodes, the higher the ion concentration in the extract will be, and this becomes toxic to cells above a certain level.

In our immersion test, the weight loss and hydrogen evolution of Mg-2Zn-1Mn were found to be at a low level, and the pH value changed little (Figs. 2–4). The concentrations of Mg^{2+} and Zn^{2+} in the medium extract were also the lowest among the four sets of alloys (Fig. 7), indicating a slow corrosion rate. Therefore, only Mg-2Zn-1Mn was nontoxic to cells at 100% extraction solution. Although Mg-3Zn-1Y also had a similar weight loss and hydrogen evolution curve to Mg-2Zn-1Mn, its corrosion caused a significant increase in the pH value of the soaking medium. After 14d immersion in Ringer's solution, the pH value reached 9.3 (Fig. 3), and after 3d immersion in the medium, the pH value reached 9.0 (Table 3). A high pH value is not conducive to cell growth and metabolism [43].

4.4. In vivo *biocompatibility and osteogenetic effects*

We observed no obvious rejection reactions, allergic reactions, local or systemic toxic reactions during the 12 w period of Mg-2Zn-1Mn implantation in the humerus of the New Zealand rabbits, and we also observed no obvious pathological changes in the tissue sections of their organs at each time period referenced above (Sup. 2–5). These results show that the implanted Mg-2Zn-1Mn alloy had good biocompatibility.

Under physiological conditions, the content of Mg^{2+} in human extracellular fluid fluctuates within 0.5–1.05 mmol/L, and Mg^{2+} homeostasis is achieved through the coordination of intestinal absorption and renal excretion [44]. When the serum Mg^{2+} concentration is too high, it can cause muscle paralysis and respiratory distress, and cardiac depression may occur in severe cases [45]. After implantation, except that the serum concentrations of Mg^{2+}, Zn^{2+}, and Mn^{2+} in the experimental group were significantly higher than those of the control group on day 15, the ion concentrations at other times showed no significant differenced and did not exceed their normal limits, indicating that the implantation of Mg-2Zn-1Mn did not cause a significant increase of the serum concentration of Mg^{2+}, Zn^{2+}, and Mn^{2+}. Thus, the degradation rate of Mg-2Zn-1Mn alloy *in vivo* was found to be appropriate for biomedical applications.

In this study, we used gross specimen observation, X-ray, and micro-CT to analyze the bone specimens. The bending of the titanium plate in the blank control group resulted in bone enlargement and angulation malunion in the defect area, which may be due to the fact that the humerus is a load-bearing bone. Since the bone defect was completely detached,

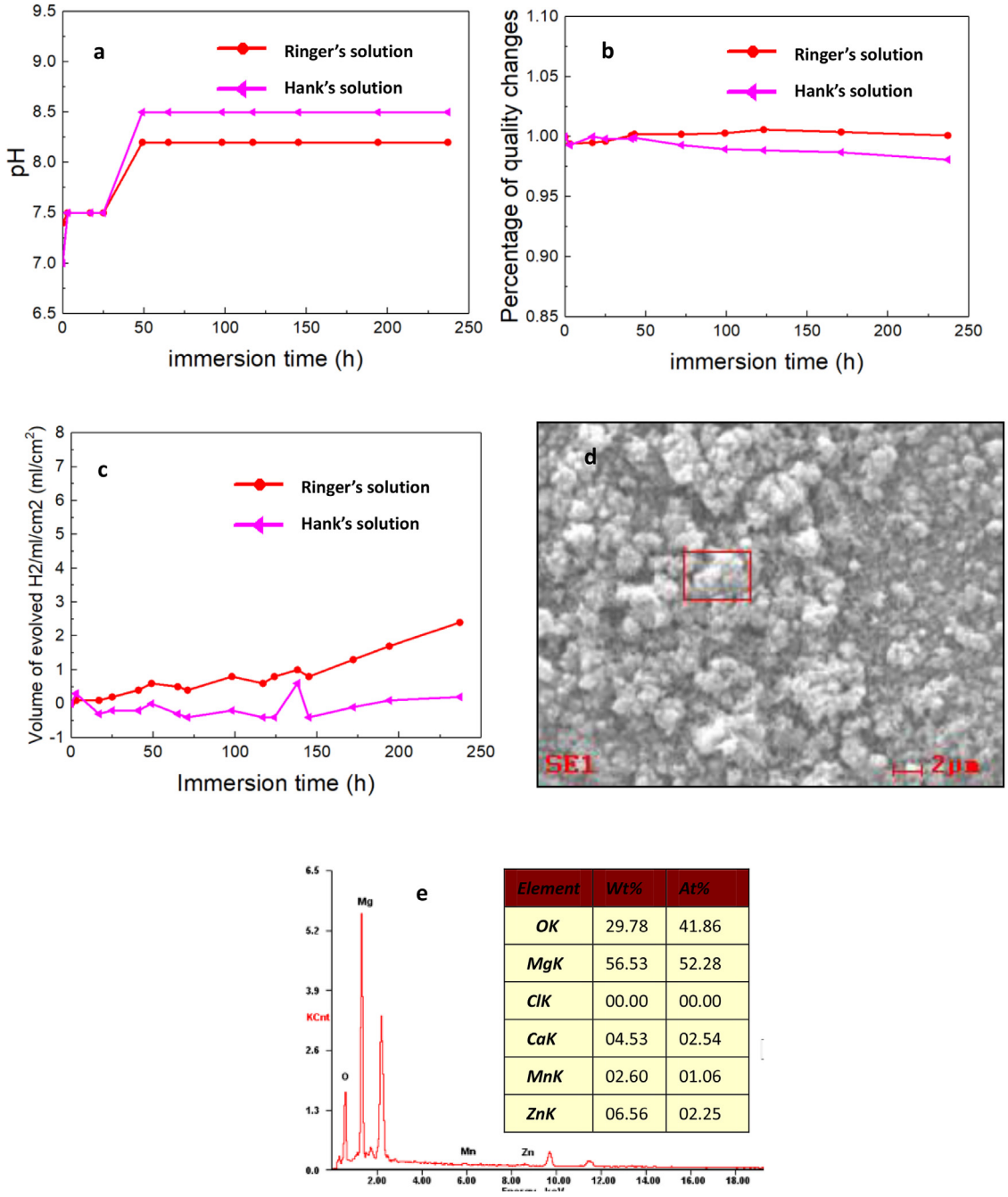

Element	Wt%	At%
OK	29.78	41.86
MgK	56.53	52.28
ClK	00.00	00.00
CaK	04.53	02.54
MnK	02.60	01.06
ZnK	06.56	02.25

Fig. 14. the immersion test results, SEM morphology and EDS energy spectrum analysis of Mg-2Mn-1Zn with Ringer's solution and Hank's solution after 240 h of corrosion. (a) pH value change; (b) weight change; (c) volume of evolved H_2; (d) SEM morphology after 240 h of corrosion in Hank's solution, and (e) EDS energy spectrum analysis after 240 h of corrosion in Hank's solution.

the unilateral titanium plate could not be affixed well. The movement of the broken end of the bone evidently deformed the titanium plate. In the implanted group, Mg-2Zn-1Mn provided partial support and limited the movement of the broken end of the bone. As a result, the bone defect healed well in the implantation group, and the bone appearance was nearly identical to that of normal rabbits. The Mg-2Zn-1Mn samples degraded gradually with the surrounding bone formation without adverse reactions or obvious subcutaneous emphysema, which indicates that the Mg-2Zn-1Mn alloy had good biocompatibility, and the rate of degradation *in vivo* was matched with the rate of new bone formation.

In the blank control group, the bone cortex of the defect area was irregular and the bone density was low, while in the implant group, the defect area was smoothly connected with the cortical bone of the two broken ends, and the bone density was similar to normal bone, indicating that Mg-2Zn-1Mn could promote bone formation. This is likely because Mg^{2+} can increase expression of $\alpha 5\beta 1$ integrin receptor and extracellular matrix protein type I collagen, promoting the ad-

hesion of human-bone-derived cells (HBDC) [46]. In addition, material degradation produced Zn^{2+}, which is a cofactor of some enzymes in bone and cartilage and plays a role in promoting bone formation as well [47]. Moreover, degradation of materials increases the local pH value, which is conducive to calcium binding [48], and Mg^{2+} in an alkaline environment can increase the expression of bone morphogenetic protein 2 (BMP-2) in the surrounding tissues, enhance the activity of osteoblasts, and promote local bone regeneration.

However, excessive increase in pH value is not conducive to cell survival and activity, and can lead to excessive secretion of local BMP-2, activate osteoclasts, and cause bone resorption [49]. In the *in vitro* corrosion experiment, although the pH value of the extract of Mg-2Zn-1Mn alloy was relatively low to begin with, it also reached 8.5 after a few days. However, we observed no obvious bone resorption around the implanted sample during the *in vivo* implantation experiment. It may be that there is a perfect buffer pair *in vivo*, which has a better buffer effect than Ringer's solution and *in vitro* medium and makes the local pH value tend toward stability. Furthermore, blood and body fluids in the organism are always circulating, and alkaline substances are quickly transported to the rest of the body and diluted sufficiently to avoid a significant increase in overall pH value. Amino acids, proteins, and other organic substances in blood and body fluids in organisms can be attached to the surface of implanted samples to play a protective role as well. Therefore, we find a solid theoretical backing that the implantation of Mg-2Zn-1Mn can promote the formation of new bone by increasing the expression of endogenous bioactive substances, which aligns with our experimental results. In addition, the buffering of pH value by the microenvironment *in vivo* and the protection of some organic compounds on the sample surface may also indirectly accelerate the repair of bone defects. In general, we find that Mg-2Zn-1Mn has excellent *in vitro* and *in vivo* biocompatibility.

5. Conclusion

In this study, we prepared Mg-3Zn, Mg-3Zn-1Y, Mg-2Zn-1Mn and Mg-2.5Y-2.5Nd alloys by the casting extrusion method. Our mechanical properties test indicated that they all have similar mechanical properties to human bone, and our *in vitro* corrosion experiments showed that the corrosion resistance of Mg-2Zn-1Mn is better than the other three magnesium alloys. Cytotoxicity tests demonstrated that Mg-2Zn-1Mn had no cytotoxicity, while Mg-3Zn, Mg-3Zn-1Y, and Mg-2.5Y-2.5Nd alloys all had different degrees of cytotoxicity. *In vivo* implantation experiments also showed that Mg-2Zn-1Mn has good biocompatibility and the ability to promote bone formation. Therefore, Mg-2Zn-1Mn could have promising potential in the field of biomedical materials.

Acknowledgments

This work was supported by the Hunan Provincial Science and Technology Department Project (2015WK3012) and the National Natural Science Foundation of China (No. 81571021). R&D of Key Project of Hunan Provincial Science and Technology Department (2022SK2010). R&D of Key Technology of Light Metal Air Battery, Transformation and Industrialization of Scientific and Technological Achievements of Hunan Province (2020GK2071). R&D of Key Technology and Materials of Magnesium Air Battery, Transformation of Scientific and Technological Achievements of Changsha City (Kh2005186). And Technology Fundation (2021-JCJQ-JJ-0432).

Supplementary materials

Supplementary material associated with this article can be found, in the online version, at doi:10.1016/j.jma.2022.06.010.

References

[1] K. Bardsley, A. Kwarciak, C. Freeman, et al., Biomaterials 112 (2017) 313–323.
[2] Y. Lai, Y. Li, H. Cao, et al., Biomaterials 197 (2019) 207–219.
[3] T.W. Bauer, G.F. Muschler, Clin. Orthop. Relat. Res. 371 (2000) 10–27.
[4] H.S. Han, S. Loffredo, I. Jun, J. Edwards, Y.C. Kim, H.K. Seok, F. Witte, D. Mantovani, S. Glyn-Jones, Mater. Today 23 (2019) 57–71.
[5] B. Jia, H. Yang, Z. Zhang, et al., Bioact. Mater. 6 (6) (2021) 1588–1604.
[6] R. Song, M. Murphy, C. Li, K. Ting, C. Soo, Z. Zheng, Dev. Ther. 12 (2018) 3117–3145.
[7] C.M. Rice, E.A. Mallam, A.L. Whone, P. Walsh, D.J. Brooks, N. Kane, S.R. Butler, D.I. Marks, N.J. Scolding, Clin. Pharmacol. Ther. 87 (2010) 679–685.
[8] D. He, P. Liu, X. Liu, X. Chen, F. Ma, W. Li, C. Zhao, J. Tu, J. Wuhan Univ. Technol. Mater. Sci. Ed. 29 (2014) 398–400.
[9] Y.F. Zheng, X.N. Gu, F. Witte, Mater. Sci. Eng. R Rep. 77 (2014) 1–34.
[10] M. Prakasam, J. Locs, K. Salma-Ancane, D. Loca, A. Largeteau, L. Berzina-Cimdina, J. Funct. Biomater. 8 (2017) 44.
[11] D. Pierson, J. Edick, A. Tauscher, E. Pokorney, P. Bowen, J. Gelbaugh, J. Stinson, H. Getty, C.H. Lee, J. Drelich, J. Goldman, J. Biomed. Mater. Res. B Appl. Biomater. 100 B (2012) 58–67.
[12] E.R. Shearier, P.K. Bowen, W. He, A. Drelich, J. Drelich, J. Goldman, F. Zhao, ACS Biomater. Sci. Eng. 2 (4) (2016) 634–642.
[13] C. García-Mintegui, L.C. Córdoba, J. Buxadera-Palomero, et al., Bioact. Mater. 6 (12) (2021) 4430–4446.
[14] J. Walker, S. Shadanbaz, T.B.F. Woodfield, M.P. Staiger, G.J. Dias, J. Biomed. Mater. Res. B Appl. Biomater. 102 (2014) 1316–1331.
[15] J.M. Diaz-Tocados, C. Herencia, J.M. Martinez-Moreno, A. Montes de Oca, M.E. Rodriguez-Ortiz, N. Vergara, A. Blanco, S. Steppan, Y. Almaden, M. Rodriguez, J.R. Munoz-Castaneda, Sci. Rep. 7 (2017) 7839.
[16] S. Yoshizawa, A. Brown, A. Barchowsky, C. Sfeir, Acta Biomater. 10 (2014) 2834–2842.
[17] D. Zhao, F. Witte, F. Lu, J. Wang, J. Li, L. Qin, Biomaterials 112 (2017) 287–302.
[18] P.C. Banerjee, S. Al-Saadi, L. Choudhary, S.E. Harandi, R. Singh, Materials 12 (2019) 1–21.
[19] A.P.M. Saad, N. Jasmawati, M.N. Harun, et al., Corros. Sci. 112 (2016) 495–506.
[20] Y. Yan, H. Cao, Y. Kang, et al., J. Alloy. Compd. 693 (2017) 1277–1289.
[21] Y. Yan, X. Chu, X. Luo, et al., J. Magnes. Alloy. 9 (1) (2021) 225–240.
[22] C. Liu, X. Chen, J. Chen, et al., J. Magnes. Alloy. 9 (5) (2021) 1546–1555.
[23] V.E. Bazhenov, A.V. Li, A.A. Komissarov, et al., J. Magnes. Alloy. 9 (4) (2021) 1428–1442.
[24] J.Y. Lee, D.H. Kim, H.K. Lim, et al., Mater. Lett. 59 (29–30) (2005) 3801–3805.

[25] L.Y. Sheng, B.N. Du, Z.Y. Hu, et al., J. Magnes. Alloy. 8 (3) (2020) 601–613.
[26] L. Wang, J. Jiang, H. Liu, et al., J. Magnes. Alloy. 8 (4) (2020) 1208–1220.
[27] K. Yu, L. Chen, J. Zhao, et al., Acta Biomater. 8 (7) (2012) 2845–2855.
[28] J. Hein, K. Hartmann, Reference ranges for laboratory parameters in rabbits, Tierarztl Prax K 31 (2003) 321–328.
[29] H. Pan, Y. Ren, H. Fu, et al., J. Alloy. Compd. 663 (2016) 321–331.
[30] L. Gao, R.S. Chen, E.H. Han, J. Alloy. Compd. 481 (1–2) (2009) 379–384.
[31] S. Nayak, B. Bhushan, R. Jayaganthan, et al., J. Mech. Behav. Biomed. Mater. 59 (2016) 57–70.
[32] D. Liu, Y. Ding, T. Guo, et al., Biomed. Mater. 9 (1) (2014) 015014.
[33] W. Jin, G. Wu, H. Feng, et al., Corros. Sci. 94 (2015) 142–155.
[34] R. Zeng, J. Zhang, W. Huang, et al., Trans. Nonferr. Met. Soc. China 16 (2006) s763–s771.
[35] W.A. Anderson, H.C Stumpf, Corrosion 36 (4) (1980) 212–213.
[36] O. Lunder, T.K. Aune, K. Nisancioglu, Corrosion 43 (5) (1987) 291–295.
[37] F. Rosalbino, S. De Negri, A. Saccone, et al., J. Mater. Sci. Mater. Med. 21 (4) (2010) 1091–1098.
[38] L. Gao, R.S. Chen, E.H. Han, J. Alloy. Compd. 472 (1–2) (2009) 234–240.
[39] W. Jin, G. Wu, H. Feng, et al., Corros. Sci. 94 (2015) 142–155.
[40] Y. Ding, C. Wen, P. Hodgson, et al., J. Mater. Chem. B 2 (14) (2014) 1912–1933.
[41] P. Li, C. Schille, E. Schweizer, et al., Acta Biomater. 98 (2019) 235–245.
[42] W. Jin, G. Wu, H. Feng, et al., Corros. Sci. 94 (2015) 142–155.
[43] S.C. Minocha, PH of the medium and the growth and metabolism of cells in culture[M], in: Cell and Tissue Culture in Forestry, Springer, Dordrecht, 1987, pp. 125–141.
[44] Randall, H. T, Fluid, electrolyte, and acid-base balance, The Surgical clinics of North America 56 (1076) 1019-1058.
[45] D. Attygalle, N. Rodrigo, Anaesthesia 57 (8) (2002) 778–817.
[46] H. Zreiqat, C.R. Howlett, A. Zannettino, et al., J. Biomed. Mater. Res. 62 (2) (2002) 175–184 An Official Journal of The Society for Biomaterials, The Japanese Society for Biomaterials, and The Australian Society for Biomaterials and the Korean Society for Biomaterials.
[47] E.W. Bradley, L.R. Carpio, A.J. Van Wijnen, et al., Physiol. Rev. 95 (4) (2015) 1359–1381.
[48] F.A. Exterkate, Appl. Environ. Microbiol. 66 (5) (2000) 2021–2028.
[49] H. Kaneko, T. Arakawa, H. Mano, et al., Bone 27 (4) (2000) 479–486.